RESEARCH PAPER

LAND USE/LAND COVER CHANGE WITH IMPACT ON LAND SURFACE TEMPERATURE: A CASE STUDY OF MKDA PLANNING AREA, WEST BENGAL, INDIA

Samrin Fatema[1*], Dr. Abhisek Chakrabarty[1]
[1]Vidyasgar University, Remote Sensing & GIS Department, Midnapore, 721102, India
*Corresponding author: asamrin1@gmail.com
Received: March 31th, 2019 / Accepted: November 20th, 2020 / Published: December 31st, 2020
https://DOI-10.24057/2071-9388-2020-62

ABSTRACT. The type of surface influences the temperature of a surface. If it is made of concrete or another hard material, the temperature will be higher. Hence it is essential to study the land surface temperature (LST) of urban areas. The LST is an important parameter in the estimation of radiation budgets and heat balance and is a controlling factor of dynamic climate changes. In this work, we made an effort to identify the LST of the Midnapore Kharagpur Development Authority planning region. Multi-temporal images acquired by Landsat 7 ETM+, Landsat 5 TM and Landsat 8 using OLI sensors on 3 May 2001, 7 May 2011 and 29 May 2019, respectively, were corrected for radiometric and geometric errors and processed to extract LULC classes and LST. Thermal remote sensing can be used to monitor the temperature and local climate of urban areas. This study has shown that the temperature varies across the surface according to land use. It was found that the urbanized area increased from 6.79% (40.39 sq. km) to 11.6% (69.2 sq. km) between 2001 and 2011 and from 11.6% (69.2 sq. km) to 17.22 % (102.79 sq. km) between 2011 and 2019. The LST study has shown that there has been a tremendous change in the spatial pattern of the temperature between 2001 and 2019. Whereas in 2001 the highest temperature did not exceed 34°C, by 2019 it had increased by nearly 8°C, reaching 41.29°C. So, the findings of this study are significant.

KEY WORDS: LULC, Change detection, LST, Thermal Remote sensing, GIS

CITATION: Samrin Fatema, Dr. Abhisek Chakrabarty (2020). Land Use/Land Cover Change With Impact On Land Surface Temperature: A Case Study Of Mkda Planning Area, West Bengal, India. Geography, Environment, Sustainability, Vol.13, No 4, p. 43-53 https://DOI-10.24057/2071-9388-2020-62

ACKNOWLEDGEMENTS: The authors would like to thank the Department of Remote Sensing and GIS, Vidyasagar University for providing the necessary infrastructural facility to carry out the research.

Conflict of interests: The authors reported no potential conflict of interest.

INTRODUCTION

The land surface temperature (LST) is the temperature of the earth's surface. The LST varies with Land Use Land Cover (LULC) type. It is a result of the energy and water balance of the earth's surface at the global and regional levels (Rozenstein et al. 2014). It gives information about the surface energy changes with time. This is an important parameter for monitoring vegetation, global warming and changes in built-up area. Currently, the LST is a significant environmental issue (Kayet et al. 2016). The temperature is increasing across the world daily because of the greenhouse gas effect, the ozone hole, etc. Scientists need to concentrate on studying the LST to reduce the impacts of global climate change. Hence, more research is required in this field. Various studies have been carried out on estimating the LST using thermal remote sensing (Southworth 2004). The first remotely sensed thermal images were obtained in 1960 from the NOAA satellite TIROS II with a very low resolution. In 1984, NASA launched the first operational satellite mission with a thermal camera (Landsat 4 TM), which covered the 10.5–12.5 µm spectrum with a resolution of 60–120 m. In 2013, NASA launched Landsat 8, with an enhanced thermal infrared (TIRS) camera. This had two bands (bands 10 and 11), covering the thermal spectrum (10.6–12.5 µm). Atmospheric correction was carried out using the split-window technique (Reuter et al. 2015). Landsat is still the only mission with more than 30 years of archived imagery, including thermal infrared imagery (Wan & Li 2010). Kustas & Anderson, 2009 utilized thermal infrared remote sensing to model land surfaces. Remote sensing and GIS techniques can be used to detect land use change and its impact on the LST (Latif S. 2014). Fu & Weng (2016) and Lv & Zhou (2011) used the Landsat thermal band to estimate the surface energy of an urban area and generate a land use change map. Alavipanah et al. (2007) used remote sensing techniques and Landsat thermal data to produce a temperature map of the Yardang region of the Lut Desert (Iran). Satiprasad (2013) created a methodology to determine the activity of land use change in the surface temperature in Howrah city. Heat islands are formed in the air above urban areas due to the heat absorbed and discharged by buildings, concrete structures and other impervious surfaces, which act as inactive vaults (Renssen et al. 2005). The LST is a vital climate variable related to climate change and is an exponent of the energy balance at the surface. It plays a key role in the physics of the land surface processes (James &

Mundia 2014). Saradjian and Jouybari-Moghaddam (2019) developed a method to retrieve the land surface emissivity (LSE) and LST simultaneously from Landsat 8 images. Li and Jiang (2018) estimated the LST using a generalized split-window (GSW) algorithm and validated it using the MOD11_L2 V6 product. Nguyen et al. (2019) derived the LST from Landsat 8 data using the split-window method. Their results showed that the LST is much higher than in the early part of the dry season. The LST and vegetation are strongly related. Temperature–vegetation plots reveal the chronological trajectory of pixels from low-temperature–high-vegetation conditions to high-temperature–low-vegetation conditions (Amiri et al. 2009). A study carried out in an urban area showed that an increase in the built-up area was accompanied by a decrease in vegetation, resulting in urban microclimatic changes (Buyadi et al. 2013). Another study revealed that the LST and vegetation are closely related. Different vegetation indices show an excess of vegetation, such as fractional vegetation cover and the normalized vegetation index (NDVI) (Amiri et al. 2009). A negative relation was found between the LST and NDVI. Green area affected the temperature (Jiang & Tian 2010) through soil moisture variations, LSE, albedo and vegetation type with dense vegetation reducing the temperature (Chen et al. 2000). Both the LST and surface imperviousness (SI) can be derived from satellite imagery. The temperatures of non-urban areas are lower than those of urban areas (White-newsome et al. 2013).

In this study, we attempted to calculate changes in the LST using thermal remote sensing and GIS. As we all know, the use of remote sensing and GIS is a powerful technique for acquiring temporal and spatial information within a narrow time span. This methodology allows to detect LULC change. Two major urban patches and a suburban-rural area were studied. The primary objectives of this study were (1) to extract and calculate the LST of the present study area during three timespans and (2) to analyse the LULC changes in relation to the changes in the LST.

STUDY AREA

The area under the Midnapore Kharagpur Development Authority (Fig.1) is situated in Paschim Medinipur District of West Bengal, India. It was formed in 2003 with the basic aim of controlling land use and development by preventing haphazard growth within the planning area. The authority has a total planning area of 596.76 sq. km, consisting of 464 mouzas (cadastre). The area consists of 14 gram-panchayats (GP) of Medinipur, Kharagpur-I, Kharagpur-II, Salboni Block and 54 wards of Kharagpur and Medinipur municipal areas. The study area extends between 87º09´00´´E and 87º28´00´´E and between 22º14´00´´N and 23º34´00´´N, it has several stretches of agricultural land and many industries that are situated in the Kharagpur Municipality (Fatema, & Chakrabarty 2017). The Kangsabati is the only perennial river of the study area. It flows almost in the middle of the Midnapore Kharagpur Development Authority area. Besides, there is an important stream within the Midnapore town, known as the 'Dari Bandh Khal', which has a south-easterly course. It joins the river Kasai and contributes to the system's internal drainage. The elevation of the study area varies between 20 m and 60 m above mean sea level.

MATERIALS AND METHODS

Three sets of remotely sensed data for path 139, row 44, 45 (WRS-2) were downloaded from the USGS portal, including data from Landsat 5, Landsat 7 and Landsat 8. The surface reflectance and brightness temperature data of these sets were processed by the Landsat Ecosystem Disturbance Adaptive Processing System (Fu & Weng 2016). Details of the dataset are provided in Table 1. Since the satellite images may still contain noisy pixels, all the images were subjected to geometric, radiometric and atmospheric correction. Also, a mosaic operation was performed to obtain the study area and the Normalized Difference Vegetation Index (NDVI) was derived from the surface reflectance.

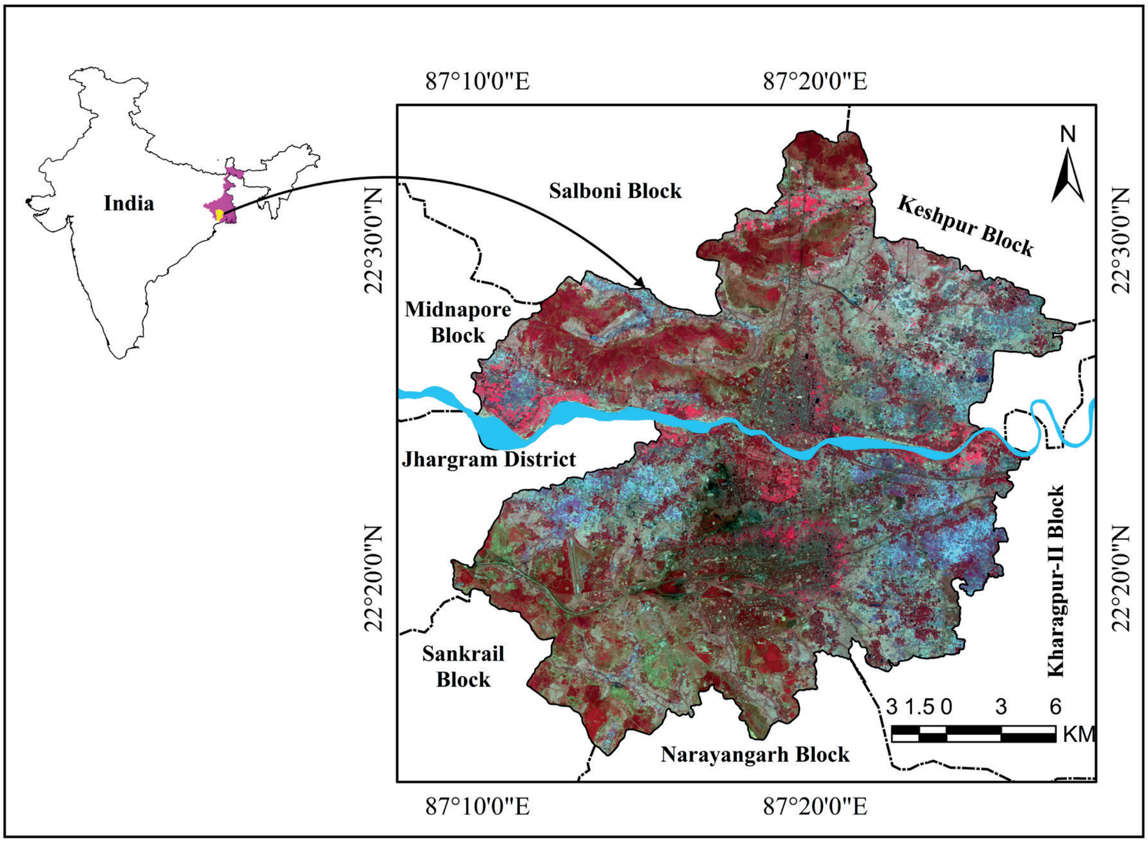

Fig. 1. Location map of the study area

LULC classification

We attempted to determine the land use land cover (Fig. 2) of our study area using remote sensing and GIS techniques. The supervised classification (maximum likelihood algorithm) method was used for identifying the LULC categories from the satellite images and the toposheet. The LULC classes (2001, 2011 & 2019) included agricultural fallow, fallow land, cultivated land, forest, river, sand, settlement, vegetation, water body and industry. The areas corresponding to different LULC classes were calculated using the pixel grid cell method (15 m×15 m) (Kayet et al. 2016). The LULC feature category was identified based on visual interpretation of the satellite imagery and the information on the actual LULC. The LULC nomenclature is presented in Table 2.

Maximum likelihood classification

A lot of research has been conducted in the field of satellite image classification, both parametric and nonparametric. We chose the maximum likelihood classifier, which uses a parametric method. This is the most popular method used to classify satellite images. It essentially uses Bayes' theorem. It is based on the use of a discriminant function to fix the pixel that belongs to the highest likelihood class (Ahmad & Quegan 2012). Maximum likelihood classification was performed using Equation 1. The accuracy (Kappa coefficient) of a classification process is usually assessed by comparing the results of classification against data obtained from field visits, high-spatial-resolution images or toposheets (Bokaie et al. 2016).

Table 1. Data used of the present study

Data	Sensor	Date	Band	Resolution (Thermal)	Path/Row
Landsat 7	ETM	3rd May 2001	6	60 (30)	139/44,45
Landsat 5	TM	7th May 2011	6	120 (30)	139/44,45
Landsat 8	OLI TIRS	29th May 2019	10/11	100	139/44

Table 2. Land use and land cover (LULC) nomenclature

LULC Classes	Land Use Included in This Class
Agriculture Fallow (AF)	Non-irrigated lands
Fallow land (FL)	Ready for construction, real-estate plots, open area
Cultivated Land (CL)	Irrigated lands
Forest	Open Forest, Dense Forest, Protected forest
River	River
Sand	Sand
Settlement (Sett)	Built-up area
Vegetation (Veg)	Plantation and Shrub
Water Body (WB)	Reservoir, Ponds, Open water
Industry (Indus)	Industrial area

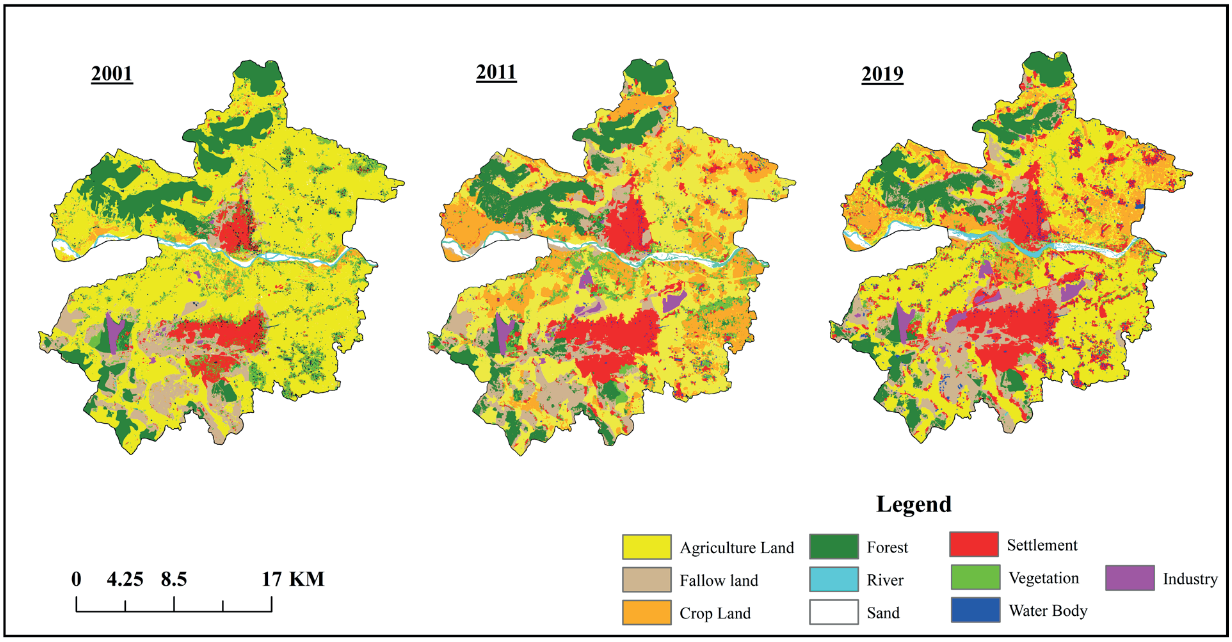

Fig. 2. Spatio-temporal pattern of land transformation

$$Lk(X) = \frac{1}{(2\pi)\frac{n}{2}\left|\Sigma_k\right|\frac{1}{2}} \exp\left(-\frac{1}{2}(X-\mu_k)\sum_k^{-1}(X-\mu_k)^t\right) \tag{1}$$

where
n is the number of bands,
X is the image data of bands n,
Lk (X) is the likelihood of X belonging to class k,
μk is the mean vector of class k,
∑k defines the variance-covariance matrix of class k and
|Σk| is the determinat of Σk.

Determination of kappa coefficient

An accuracy assessment plays a significant role in the analysis of the resultant classes after the classification process. The Kappa index (Table 5) is a method that is used widely to measure the accuracy of the assessment of a remotely sensed image (Conglaton, 1991). The Kappa coefficient is considered to be more robust than the simple overall accuracy because it takes into account the proportion of pixels that have been classified correctly merely by chance. A confusion (error) matrix was used to represent the accuracy assessment (Lillesand et al. 1994) using random sampling methods. The Kappa coefficient was computed as follows (Conglaton 1991):

$$KA = \frac{na - s}{n^2 - s} \tag{2}$$

where
KA = Kappa coefficient,
n = number of ground points in the error matrix (the sum of all r individual cell values),
a = sum of diagonal segments and
s = sum of row and column.

Determination of land surface temperature

The TIR band (band 6 of Landsat 5 and 7 and band 10/11 of Landsat 8 OLI) records the radiation with the spectral range between 10.4 µm and 12.5 µm, which is emitted by the surface of the earth (Buyadi et al. 2013). The LST plays a vital role in environmental processes and provides basic information on the earth surface biophysical properties and climate. For example, Landsat 7 ETM+ data can be used to estimate radiation budgets in heat balance studies and as a control for climate models (Mallick, Kant and Bharath 2008). In most of the research, the LST is generated using digital image processing software and GIS software. In this study, the ArcGIS 10.3 and ERDAS Imagine software packages were used to generate LST maps. The methodology developed for the LST mapping is shown in Fig. 3.

Thermal map generation

The remotely sensed data were acquired and stored in a binary format. The values ranged between 0 and 255. Thermal remote sensing can convert the data from digital numbers to radiance values. The thermal energy responses of various landforms reveal the variations in the temperatures of different surfaces. In this study, the surface temperature was extracted from the thermal bands 6, 6.1, 10 and 11 of Landsat ETM+, TM, and OLI_TIRS data.

Computation of the NDVI

The NDVI is widely used in LST studies because it is less sensitive to changes in atmospheric conditions compared with other indices. The NDVI is a numerical indicator of live green vegetation. It is derived from the near-infrared and visible bands of the electromagnetic spectrum. The range of NDVI values is from -1 to 1. In this study, the NDVI was used to represent the relationship between the vegetation and LST. The NDVI can be obtained using the following equation:

$$NDVI = \frac{NIR -}{NIR +} \tag{3}$$

The NIR and red bands of Landsat 5–7 {(Band 4 – Band 3)/(Band 4 + Band 3)} and Landsat 8 {(Band 5 – Band 4)/(Band 5 + Band 4)} were used in this study. NDVI maps were generated using the ERDAS Imagine software package (Version 14).

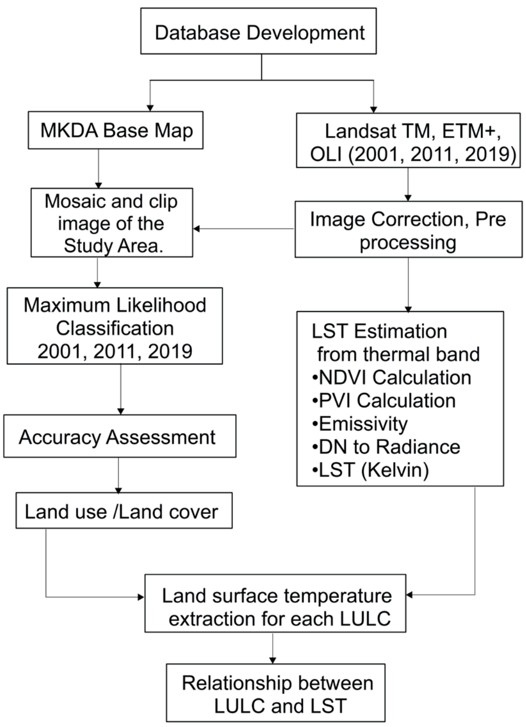

Fig. 3. Methodology flow diagram of the study

Computation of land surface temperature LST

The thermal infrared bands of the Landsat images (band 6 of Landsat 5 and 7, bands 10 and 11 of Landsat 8 OLI, with spatial resolution of 30 m) were used to calculate the LST of the MKDA planning area. The LST was derived as described in the following sections.

Calculation NDVI and Proportional Vegetation Index

The land surface emissivity (LSE) was derived from the NDVI. The PVI value was calculated as:

$$Pv = \left(\frac{NDVI - NDVImin}{NDVImax - NDVImin}\right)2 \quad (4)$$

where Pv is the proportion of vegetation.

Calculation of Emissivity

The NDVI threshold can be used to calculate the emissivity using the following formula (Guha, Govil and Diwan 2020) & (Baba 2016):

$$\varepsilon = 0.004 * Pv + 0.986 \quad (5)$$

The value of NDVI ranges between -1 and 1. When the NDVI value crossed this range (-1 to 1), the corresponding LSE value was used (Anandababu D et al. 2018).

DN to Radiance

The digital numbers (DN) of the Landsat 7 and 5 data for 2001 and 2011 were converted to spectral radiance (L) values (USGS, 2001) using Equation 6. Similarly, Equation 7 was used for the Landsat 8 OLI_TRS data of 2019. The values obtained using these equations are presented in Table 3.

Landsat 5/7
Landsat 8

$$L\lambda = \frac{L_{max} - L_{min}}{Qcal_{max} - Qcal_{min}} * (Qcal - Qcal_{min}) + L_{min} \quad (6)$$

$$L\lambda = M_L Q_{cal} + A_L \quad (7)$$

where
Lλ = spectral radiance,
Qcal = quantized and calibrated standard product pixel value (DN),
L_{min} = spectral radiance scaled to Qcalmin,
L_{max} = spectral radiance scaled to Qcalmax,
$Qcal_{min}$ = minimum quantized calibrated pixel value,
$Qcal_{max}$ = maximum quantized calibrated pixel value,
M_L = band specification multiplicative rescale factor (Radiance _Add_Band_X) and
A_L = band specification additive rescale factor (Radiance _ Add_Band_X) (USGS, 2001).

Compute Land Surface Temperature (Kelvin)

The spectral radiance (Lλ) values of Landsat 7 and 5 of the years 2001 and 2011 were converted to the temperatures (in Kelvin) (USGS, 2001) using Equation 8. Similarly, the Landsat 8 OLI_TRS data for the year 2019 were converted using Equations 8 and 9. The values obtained using these equations are presented in Table 4.

Landsat 5/7

$$BT = \frac{K2}{\left(\frac{k1}{L\lambda} + 1\right)} \quad (8)$$

Landsat 8

$$T = \frac{BT}{\left[1 + (\lambda * BT / c2) * \ln(e)\right]} \quad (9)$$

where
BT = at-satellite brightness temperature (K),
T = Brightness temperature to land surface temperature (K),
λ = wavelength of emitted radiance (Landsat 8 Band 10 = 10.60 – 11.19, Band 11 = 11.50 – 12.51),
Lλ = DN-to-radiance conversion value,
K1 = band-specific thermal conversation constant (K1_ Constant _Band_x),
K2 = band-specific thermal conversation constant (K2_ Constant _Band_x),
c2 = h*c/s = 1.4388* 10-2 m K = 14388 μm,
e = emission,
h = Planck's constant = 6.626176*10-34 J s,
s = Boltzmann constant =1.38*10-23 J/K and
c = velocity of light = 2.998*108 m/s.

Converted Kelvin to Centigrade

The temperature in Kelvin was converted to the temperature in Celsius [19] using Equation 10

Temperature (°C) = Temperature (Kelvin) - 273.15 (10)

RESULTS

Spatio-temporal land use land cover change detection (2001, 2011 and 2019)

Several techniques are available for assessing spatio-temporal changes in the land use land cover of any

Table 3. Related value for DN to radiance conversion

Data	L_{max}	L_{min}	$Qcal_{max}$	$Qcal_{min}$	M_L	A_L
Landsat7	17.040	0.00	255	1	-	-
Landsat5	15.303	1.23	255	1	-	-
Landsat8	-	-	65535	1	3.3420E-04	0.10000

Table 4. Related value for Spectral radiance (Lλ) to temperature conversion

Data	Date	Constant 1-K1	Constant 2-K2
Landsat 7	3rd May 2001	666.09	1282.71
Landsat 5	7th May 2011	607.76	1260.56
Landsat 8	29th May 2019	774.8853 / 480.89	1321.0789 / 1201.14

area and a useful post-classification change detection technique was selected for the present study. The easiest technique was selected. Multi-sensor or multi-temporal images provide better results after reducing the atmospheric, sensor and environmental impacts (Hussain et al. 2013). In this study, reclassified fractional images of three years (2001, 2011 and 2019) were used to monitor the spatial changes in the MKDA planning area. Supervised classification method was used to generate land use land cover maps (with accuracy assessment), as shown in Table 5. The total extent of the study area was 596.76 sq. km. The proportion of agricultural land was 55% and that of active agricultural land was 11%, as indicated by the classification. Both agricultural land and active agricultural land were widely distributed throughout the planning area (Table 6). The extent of the urbanized area has increased from 6.79% (40.39 sq. km) to 11.6% (69.2 sq. km) between 2001 and 2011 and between 2011 to 2019 it has further increased up to 17.22% (102.79 sq. km). Also, the vegetation cover has decreased from 6.72% (40.08 sq. km) to 3.29% (19.63 sq. km) between the years 2001 and 2019. This is the clearest cause of the increased LST.

Retrieval of Land Surface temperature (LST)

The remote sensing technique can be used to assess and map the LST of any study area. The LST maps of May show that there has been a tremendous change in the spatial pattern of the temperature from 2001 to 2019 (Fig. 4). The details of the temperature ranges (2001, 2011 and 2019) of the area are provided in Table 7 and Fig. 5. The lowest temperatures (<25°C) in 2001 were mainly confined to the central and northern parts of the study area, adjacent to the river and forested areas. In the year 2011, the lowest temperature increased by almost 1°C. This temperature was mainly confined to the north-eastern part of the study area. In 2019, the minimum temperature increased by nearly 4°C (to 28.13°C) and surpassed the

Table 5. Result of the accuracy assessment of land use/land cover classification

LULC Classes	3rd May 2001		7th May 2011		29th May 2019	
	User's	Producer's	User's	Producer's	User's	Producer's
AF	81.72	96.20	67.62	86.67	67.68	95.71
FL	83.33	47.62	60.00	78.33	100	54.76
CL	66.67	50.00	57.50	50.00	89.66	54.17
Forest	94.12	94.12	83.33	100	92.00	95.83
River	0.00	0.00	100	79.87	100	100
Sand	100	100	92.31	80.00	100	75.00
Set	88.89	80.00	81.25	86.67	84.00	100
Veg	71.43	62.50	84.62	73.33	85.71	100
WB	100	50.00	100	80.00	100	100
Indus	0.00	0.00	88.24	100	100	100
Overall accuracy (%)	83.33		81.48		81.60	
Kappa Index	0.7394		0.7185		0.7718	

Table 6. Area distribution of land use/land cover classification of the study area

Class Name	2001 (sq.km)	Area %	2011 (sq.km)	Area %	2019 (sq.km)	Area %
AF	328.91	55.12	207.08	34.70	225.93	37.86
FL	62.46	10.47	70.73	11.85	80.4	13.47
CL	23.98	4.02	119.35	20.00	71.14	11.92
Forest	76.39	12.80	75.56	12.66	65.35	10.95
River	4.84	0.81	3.73	0.63	5.01	0.84
Sand	7.36	1.23	8.29	1.39	7.07	1.18
Set	40.39	6.77	69.2	11.60	102.79	17.22
Veg	40.08	6.72	29.38	4.92	19.63	3.29
WB	8.67	1.45	5.76	0.97	10.04	1.68
Indus	3.68	0.62	7.68	1.29	9.4	1.58
Total	596.76	100	596.76	100	596.76	100

highest temperature of 2001 and 2011. The LST map of May 2019 (Fig.4) shows the temperature increase in the north-eastern, south-western and western parts. The highest temperature of 2019 was not confined to built-up or urban land (Midnapore and Kharagpur municipalities). Instead, it was observed in seasonal agricultural fallow land, fallow land, industrial land and riverside sand areas. There is a remarkable similarity between the patterns of the areas where the temperature was relatively high and the areas where the surface was impervious. The low-temperature areas mainly corresponded to vegetated land. The different temperatures of the built-up area and the semi-urban regions indicate the effect of the urban heat island.

Inter-relationship between LST and each LULC classes

The present study shows that Midnapore and Kharagpur municipalities and their peripheral areas experienced rapid change during 2001–2019. The growth of urban areas was found to be closely related to LULC changes. The primary cause of these changes was the increasing population density, especially in the peri-urban areas. This change played an important role in controlling the micro-climate of the study area. The expansion of the industrial area and the built-up area affected the summer temperature, which aggravated the greenhouse effect.

It was found that that there is a trend in the LST changes over time in the study area and that it is related to the land

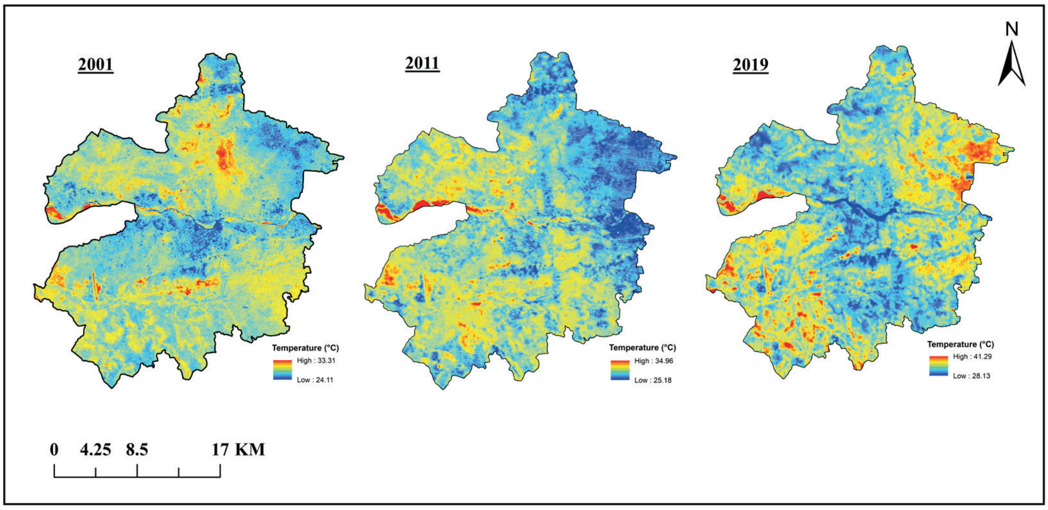

Fig. 4. Spatio-temporal pattern of LST 2001, 2011 & 2019

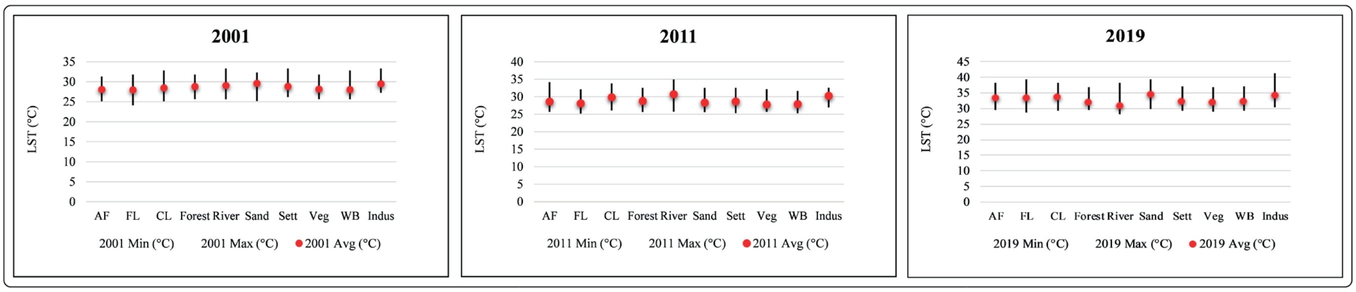

Fig. 5. LULC and the LST range 2001, 2011 & 2019

Table 7. LST for each LULC category

Class Name	3rd May 2001		7th May 2011		29th May 2019	
	Min (°C)	Max (°C)	Min (°C)	Max (°C)	Min (°C)	Max (°C)
AF	25.12	31.31	25.68	34.20	29.65	38.29
FL	24.11	31.82	25.18	32.10	28.76	39.36
CL	25.09	32.82	26.06	33.80	29.33	38.26
Forest	25.64	31.82	25.63	32.52	29.58	36.97
River	25.16	32.32	25.61	32.51	28.13	38.31
Sand	25.63	33.31	25.72	34.96	29.93	39.24
Set	26.15	33.31	25.29	32.51	29.16	37.08
Veg	25.64	31.81	25.68	32.14	29.04	36.95
WB	25.61	32.81	25.27	31.68	29.21	37.23
Indus	27.21	33.4	26.97	32.57	30.35	41.29

use and land cover categories (Fig. 6). The relationship between LULC category and LST was analyzed to identify the role of the surface type in the micro-climate. Some areas of interest (AOI) (Fig. 7) were selected to identify the relation between the LST and LULC changes. It was found that the changes in LULC from 2001 to 2019 affected the LST. The temperatures of the settlement, sand, fallow land and other categories increased gradually. The increasing trend of LST is shown in Fig. 8. It can be seen that the extent of the built-up surface (Fig. AOI 1) increased gradually, from 0.38 sq. km (2001) to 1.79 sq. km (2019). Similarly, the LST of the built-up area increased from 30.69°C (2001) to 39.31°C (2019). From Fig.8 (AOI 2) it can be seen that in 2001 in the outer part of Midnapore Municipality only small part of the area (0.72 sq. km) corresponded to settlements, but it has rapidly increased to 1.83 sq. km in 2019, while the LST also increased from 27.88°C to 39.89°C within 8 years.

In Fig. 8 (AOI 3), the most important industrial zone of the MKDA planning area is presented. In 2001 there was agricultural fallow land, but it turned into the industrial zone in 2011 (2.08 sq. km), the extent of which has gradually increased (2.14 sq. km in 2019). Similarly, the changes in the agricultural fallow land to industrial area caused the LST to change from 28.53°C (2001) to 38.52°C (2019).

Correlation between LST and NDVI

Random points were generated to show the relationship between the LST and NDVI. A negative correlation was found between LST and NDVI (Fig. 9), with R^2 = 0.1173,

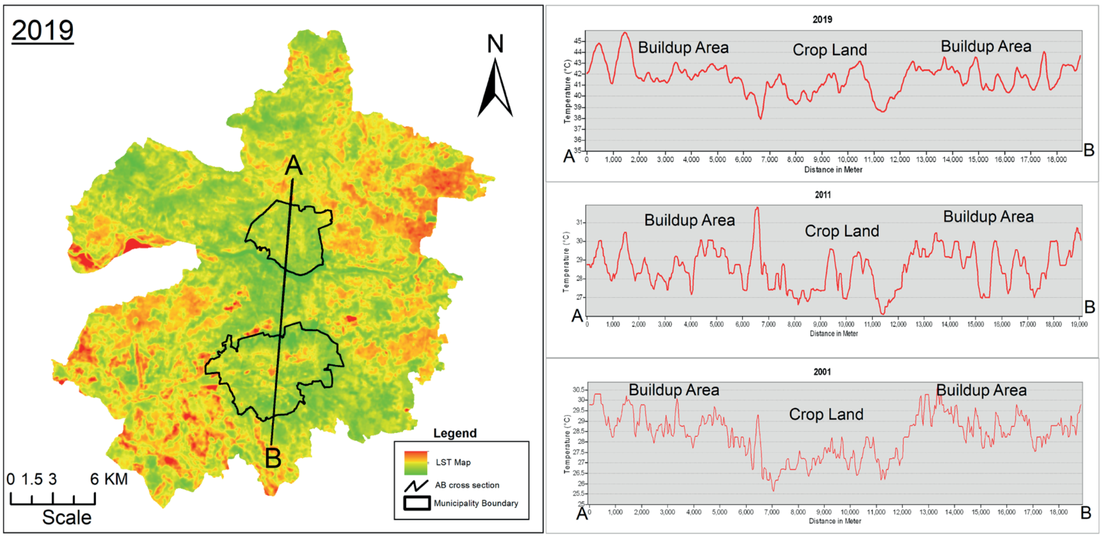

Fig. 6. LST profile of 2001, 2011 & 2019

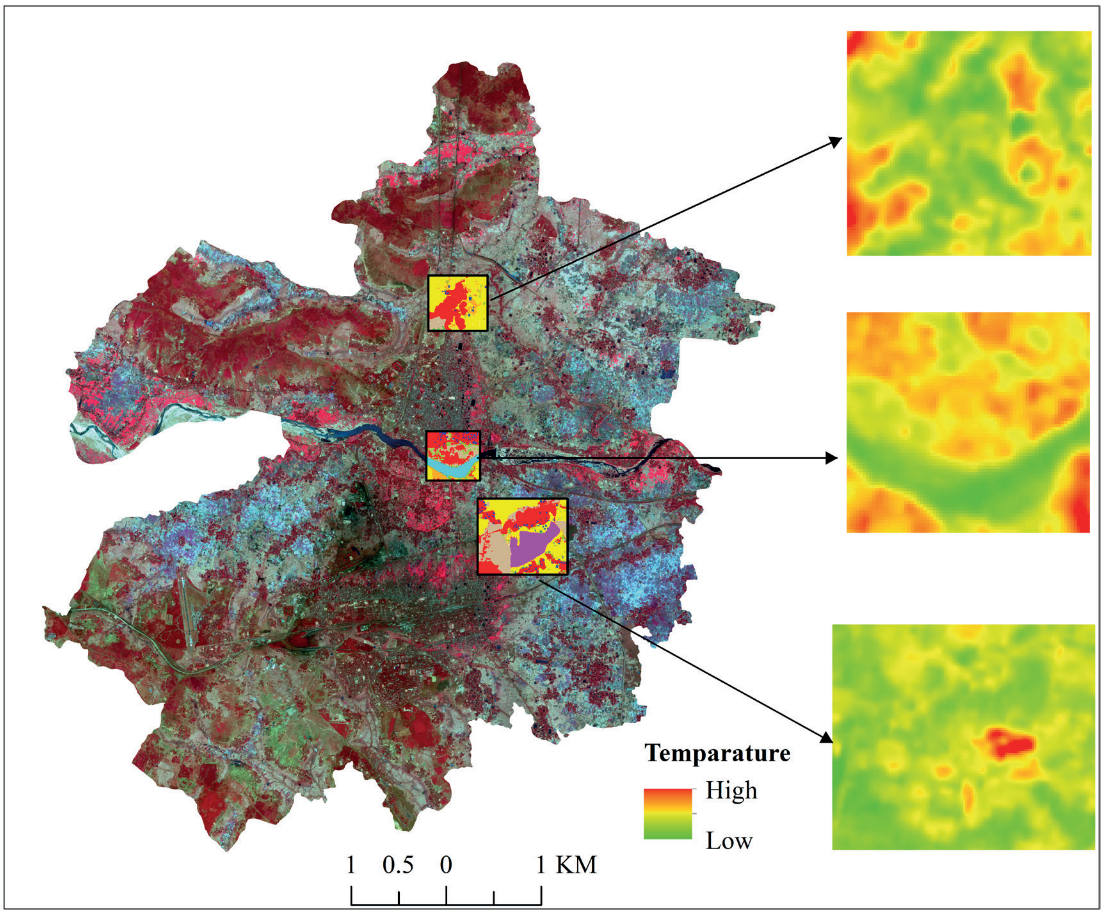

Fig. 7. Selection of the Areas of Interest

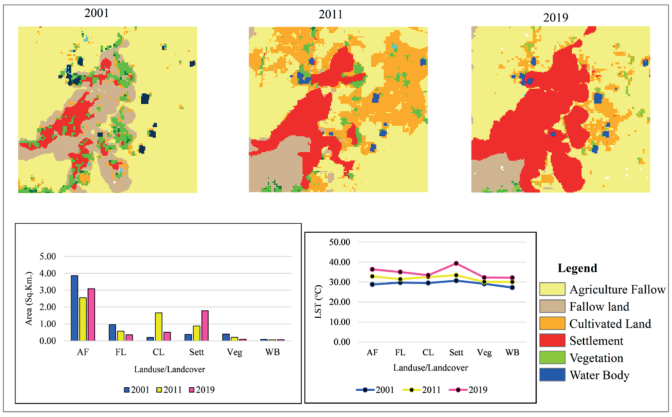

Fig. AOI 1

Fig. AOI 2

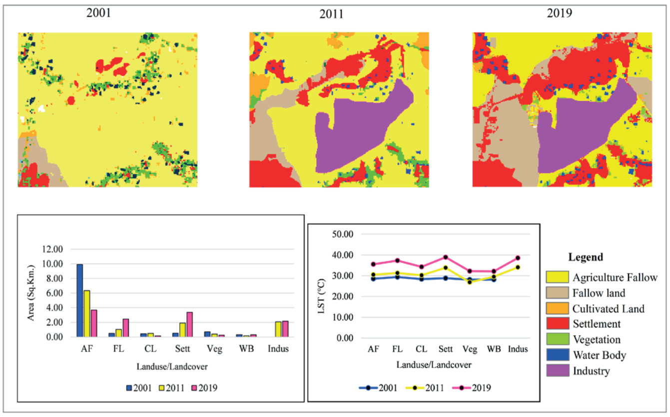

Fig. AOI 3

Fig. 8. Temporal increase of temperature in different areas over time 2001, 2011 & 2019

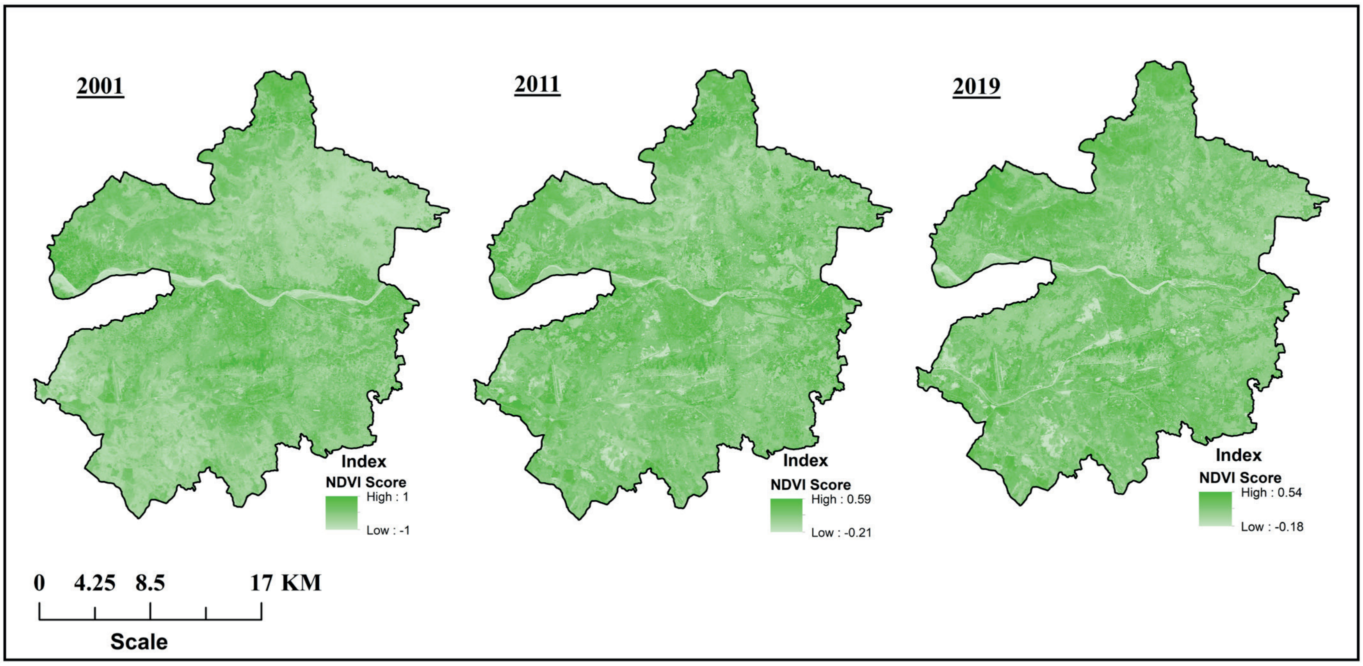

Fig. 9. NDVI classes of 2001, 2011 & 2019

0.1955 and 0.3635 in 2001, 2011 and 2019, respectively (Fig.10). The lower LST corresponded to the higher NDVI values. In 2001, the NDVI score varied between -1 and 1; in 2011 the score ranged between -0.21 and 0.59 and in 2019 it increased and ranged between -0.18 and 0.54. So, it can be said that the LST increased in the urban area over time. The results indicate that the relation between NDVI and LST is negative, with the R2 value of 0.1173 in 2001, which increased to 0.3635 in 2019.

CONCLUSIONS

Remote sensing techniques were used in this study to identify the spatio-temporal pattern of the LULC change and how this pattern impacts the LST in the MKDA planning region. It was found that the MKDA planning area experienced significant changes between 2001 and 2019. The research area was classified into ten categories: Agriculture Fallow, Fallow Land, Cultivated Land, Forest, River, Sand, Settlement, Vegetation, Water Body and Industry. The percentage of the built-up or settlement

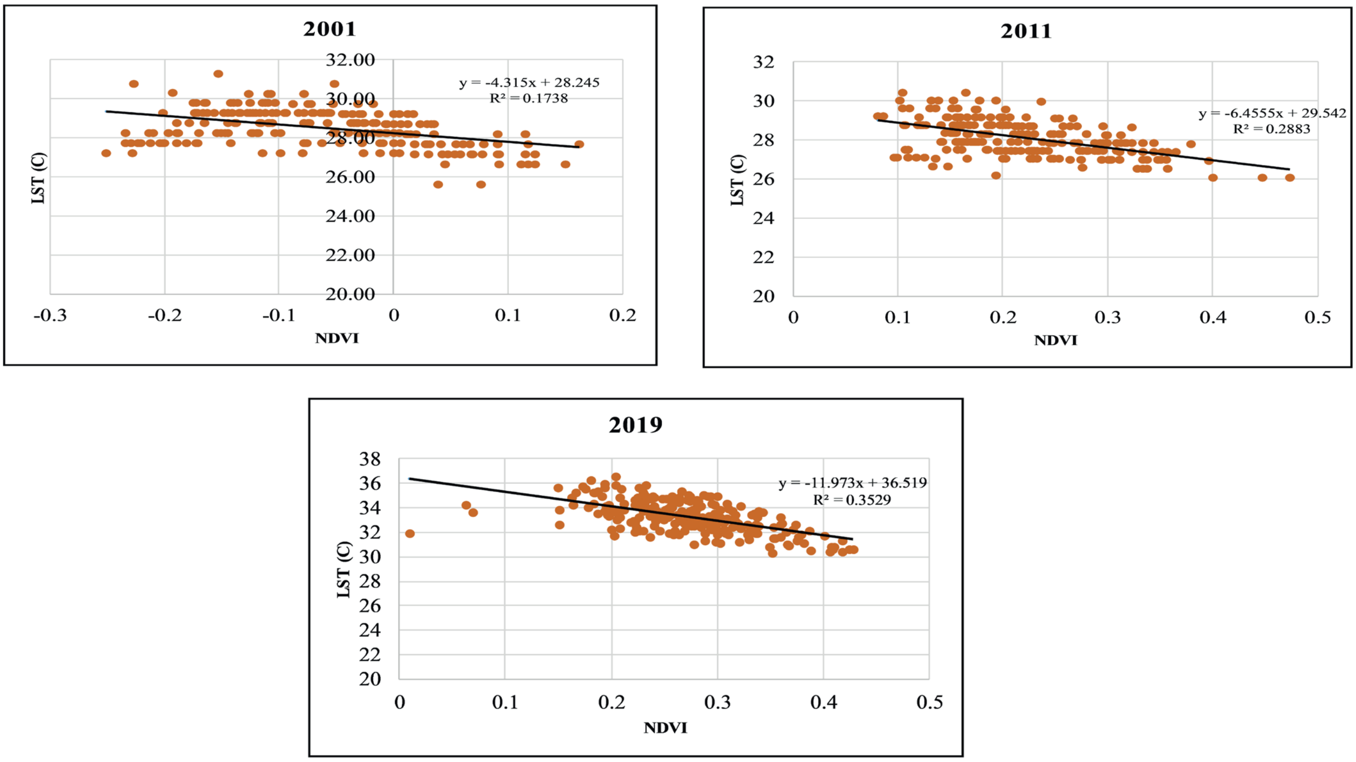

Fig. 10. Changing influence of NDVI on LST in 2001, 2011 & 2019

area increased almost three times, from 6.77% to 17.22% between 2001 to 2019. The area under this category grew particularly in the periphery of Midnapore and Kharagpur municipalities through the conversion of low-density built-up area, agricultural fallow, fallow land, etc. The extent of the industrial area and fallow land has also increased (from 0.62% to 1.58% and from 10.47% to 13.47%, respectively) through the transformation of agricultural fallow land. The extent of the forest areas and vegetation decreased by 1.85% and 3.43%, respectively. There is a strong relationship between the LULC and LST. This study found that the LST value varies depending on the LULC category. The radiant temperature in fallow land, sand and built-up areas has increased. The temperatures were higher not only in settlement or built-up areas but also in industrial areas and on riverside sand. From 2001 to 2019, the mean LST of the whole study area increased remarkably. This increasing trend of the LST can be explained by the growth of the built-up area, especially in the regions around Kharagpur and Midnapore municipalities.

REFERENCES

Ahmad A. and Quegan S. (2016). Analysis of Maximum Likelihood Classification on Multispectral Data, (January 2012).

Alavipanah S.K. et al. (2007). Land Surface Temperature in the Yardang Region of Lut Desert (Iran) Based on Field Measurements and Landsat Thermal Data, Journal Agriculture Science Technology, 9, 287-303.

Amiri R. et al. (2009). Spatial-temporal dynamics of land surface temperature in relation to fractional vegetation cover and land use/cover in the Tabriz urban area, Iran, Remote Sensing of Environment. Elsevier Inc., 113(12), 2606-2617, DOI: 10.1016/j.rse.2009.07.021.

Anandababu D., Purushothaman B. M. and Dr. S. Suresh Babu (2018). Estimation of Land Surface Temperature using LANDSAT 8 Data, INTERNATIONAL JOURNAL OF ADVANCE RESEARCH, IDEAS AND INNOVATIONS IN TECHNOLOGY, 4(2), 177-186.

Baba I.I. (2016). ESTIMATION OF LAND SURFACE TEMPERATURE OF KADUNA METROPOLIS, NIGERIA USING LANDSAT IMAGES, 11(3), 36-42.

Bokaie M. et al. (2016). Assessment of Urban Heat Island based on the relationship between land surface temperature and Land Use/Land Cover in Tehran, Sustainable Cities and Society. Elsevier B.V., 23, 94-104, DOI: 10.1016/j.scs.2016.03.009.

Buyadi S.N.A., Mohd W.M.N.W. and Misni A. (2013). Impact of Land Use Changes on the Surface Temperature Distribution of Area Surrounding the National Botanic Garden, Shah Alam, Procedia – Social and Behavioral Sciences. Elsevier B.V., 101, 516-525, DOI: 10.1016/j.sbspro.2013.07.225.

Chen S.P., Zeng S. and Xie C.G. (2000). Remote sensing and GIS for urban growth analysis in China, Photogrammetric Engineering and Remote Sensing, 66(5), 593-598, DOI: 10.1007/978-94-007-4698-5.

Congalton R.G. (1991). A Review of Assessing the Accuracy of Classifications of Remotely Sensed Data, 46 (October 1990), 35-46.

Congalton R.G. (1991). A Review of Assessing the Accuracy of Classifications of Remotely Sensed Data, 46(October 1990), 35-46.

Fatema S. and Chakrabarty A. (2020). Accident Hotspot Identification on the Midnapore Kharagpur Development Authority Planning Area, (2), 169-174, DOI: 10.35940/ijrte.B3351.079220.

Fu P. and Weng Q. (2016). A time series analysis of urbanization induced land use and land cover change and its impact on land surface temperature with Landsat imagery, Remote Sensing of Environment. Elsevier Inc., 175, 205-214, DOI: 10.1016/j.rse.2015.12.040.

Ghulam A. and Louis S. (2010). Calculating surface temperature using Landsat thermal imagery, 1-9.

Guha S., Govil H. and Diwan P. (2020). Monitoring LST-NDVI Relationship Using Premonsoon Landsat Datasets, 2020(1).

Hussain M. et al. (2013). ISPRS Journal of Photogrammetry and Remote Sensing Change detection from remotely sensed images: From pixel-based to object-based approaches, ISPRS Journal of Photogrammetry and Remote Sensing. International Society for Photogrammetry and Remote Sensing, Inc. (ISPRS), 80, 91-106, DOI: 10.1016/j.isprsjprs.2013.03.006.

James M.M. and Mundia C.N. (2014). Dynamism of land use changes on surface temperature in Kenya: a case study of Nairobi City. International Journal of Science and Research, 3(4), 38-41.

Jiang J. and Tian G. (2010). Analysis of the impact of Land use/Land cover change on Land Surface Temperature with Remote Sensing, Procedia Environmental Sciences, 2(5), 571-575, DOI: 10.1016/j.proenv.2010.10.062.

Kayet N. et al. (2016). Spatial impact of land use / land cover change on surface temperature distribution in Saranda Forest, Jharkhand, Modeling Earth Systems and Environment. Springer International Publishing, 2(3), 1-10, DOI: 10.1007/s40808-016-0159-x.

Kustas W. and Anderson M. (2009). Agricultural and Forest Meteorology Advances in thermal infrared remote sensing for land surface modeling, 149, 2071-2081, DOI: 10.1016/j.agrformet.2009.05.016.

Latif S. (2014). Land Surface Temperature Retrival of Landsat-8 Data Using Split Window Algorithm – A Case Study of Ranchi District, 2(4), 3840-3849.

Li S. and Jiang G.M. (2018). Land Surface Temperature Retrieval from Landsat-8 Data with the Generalized Split-Window Algorithm, IEEE Access. IEEE, 6, 18149-18162, DOI: 10.1109/ACCESS.2018.2818741.

Lillesand T., Kiefer R.W. and Chipman J. (2015). Remote sensing and image interpretation. John Wiley & Sons.

Lv Z. Q. and Zhou Q.G. (2011). Utility of Landsat image in the study of land cover and land surface temperature change, Procedia Environmental Sciences, 10(PART B), 1287-1292, DOI: 10.1016/j.proenv.2011.09.206.

Mallick J., Kant Y. and Bharath B.D. (2008). Estimation of land surface temperature over Delhi using Landsat-7 ETM +, (August).

Nguyen Q.K., et al. (2019). Land Surface Temperature Dynamics In Dry Season 2015-2016 According To Landsat 8 Data In The South-East Region of Vietnam, Geography, Environment, Sustainability, 12(1), 75-87, DOI: 10.24057/2071-9388-2018-06.

Renssen H., et al. (2005). Simulating the Holocene climate evolution at northern high latitudes using a coupled atmosphere-sea ice-ocean-vegetation model, 23-43, DOI: 10.1007/s00382-004-0485-y.

Reuter D.C., et al. (2015). The thermal infrared sensor (tirs) on landsat 8: Design overview and pre-launch characterization, Remote Sensing, 7(1), 1135-1153, DOI: 10.3390/rs70101135.

Rozenstein O., et al. (2014). Derivation of Land Surface Temperature for Landsat-8 TIRS Using a Split Window Algorithm, 5768-5780, DOI: 10.3390/s140405768.

Saradjian M.R. and Jouybari-Moghaddam Y. (2019). Land Surface Emissivity and temperature retrieval from Landsat-8 satellite data using Support Vector Regression and weighted least squares approach, Remote Sensing Letters. Taylor & Francis, 10(5), 439-448, DOI: 10.1080/2150704X.2019.1569273.

Satiprasad S. (2013). Monitoring urban Land use land cover change by Multi-Temporal remote sensing information in Howrah city, India, International Research Journal of Earth Sciences, 1(5), 1-6.

Southworth J. (2010). An assessment of Landsat TM band 6 thermal data for analysing land cover in tropical dry forest regions, 1161, DOI: 10.1080/0143116031000139917.

USGS (2001). Landsat 7 Science Data Users handbooks.

Wan Z. and Li Z. L. (2010). Radiance – based validation of the V5 MODIS land – surface temperature product, 1161, DOI: 10.1080/01431160802036565.

White-Newsome J.L., et al. (2013). Measurements: A Public Health Perspective, 121(8), 925-931.